

# Thermal Conductivity, Elastic Modulus, and Coefficient of Thermal Expansion of Polymer Composites Filled with Ceramic Particles for Electronic Packaging

C. P. WONG, RAJA S. BOLLAMPALLY

School of Materials Science and Engineering, Georgia Institute of Technology, Atlanta, Georgia 30332

Received 28 September 1998; accepted 19 April 1999

**ABSTRACT:** The effective thermal conductivity, elastic modulus, and coefficient of thermal expansion of epoxy resins filled with ceramic fillers like silica, alumina, and aluminum nitride were determined. The data obtained was compared with theoretical and semitheoretical equations in the literature that are used to predict the properties of two phase mixtures. It was found that Agari's model provided a good estimate of the composite thermal conductivity. The Hashin-Shtrikman lower bound for composite modulus fits the modulus data fairly well at low concentrations of the filler. Also, it was found that the coefficients of thermal expansion of the filled composites lie in between Schapery's upper and lower bounds. © 1999 John Wiley & Sons, Inc. *J Appl Polym Sci* 74: 3396–3403, 1999

**Key words:** polymer composites; thermal conductivity; elastic modulus; coefficient of thermal expansion; electronic packaging

## INTRODUCTION

Filled polymers are used in electronic packaging for device encapsulation. Encapsulation of electronic devices protects them from adverse environment and increases their long-term reliability. Traditionally, epoxy-based encapsulants are filled with silica. Silica has a low thermal conductivity of 1.5 W/mK, and hence, these encapsulants show a very poor thermal performance. As the heat dissipation requirements increase, improved thermally conducting packaging materials are required. This can be achieved by using thermally conducting fillers like alumina, aluminum nitride, etc. Modulus of elasticity and coefficient of thermal expansion (CTE) are other important properties critical to device encapsulants. The present research deals with the study of thermal

conductivity, modulus, and CTE of silica, silica-coated aluminum nitride, and alumina-filled epoxy composites. The results were compared with predictions from well-known models in literature.

## Models in Literature

### Thermal Conductivity

Maxwell pioneered in the study of the thermal conductivity of two-phase mixtures.<sup>1</sup> Using the potential theory, he obtained a relationship for the conductivity of a two-phase mixture consisting of randomly distributed and noninteracting homogeneous spheres in a homogeneous medium:

$$k_c = k_p \frac{k_m + 2k_p + 2\phi(k_m - k_p)}{k_m + 2k_p - \phi(k_m - k_p)} \quad (1)$$

where  $k_c$ ,  $k_m$ , and  $k_p$  are the thermal conductivities of the composite, matrix, and the particles (filler), respectively, and  $\phi$  is the volume fraction

Correspondence to: C. P. Wong.

*Journal of Applied Polymer Science*, Vol. 74, 3396–3403 (1999)  
© 1999 John Wiley & Sons, Inc. CCC 0021-8995/99/143396-08

of the filler. This model predicts the thermal conductivity of composites fairly well for low filler concentrations, and is not valid at high concentrations when the filler particles begin to touch each other.

Bruggeman<sup>2</sup> developed an implicit relationship between the thermal conductivities of the composite, the filler, and the matrix for dilute suspension of spheres:

$$1 - \phi = \left( \frac{k_p - k_c}{k_p - k_m} \right) \left( \frac{k_m}{k_c} \right)^{1/3} \quad (2)$$

Agari and Uno<sup>3</sup> developed a new model based on the generalization of models for series and parallel conduction in composites:

$$k_c = \left[ \frac{k_p^{C_2}}{C_1 k_m} \right]^\phi (C_1 k_m) \quad (3)$$

which can be rearranged as

$$\log k_c = \phi C_2 \log k_p + (1 - \phi) \log(C_1 k_m) \quad (4)$$

where  $C_1$  and  $C_2$  are experimentally determined constants.  $C_1$  is a measure of the effect of particles on the secondary structure of the polymer, and  $C_2$  is a measure of ease with which the particles begin to form conductive chains.

**Modulus of Elasticity**

There have been a number of theoretical approaches to predict the modulus of two-phase composites the simplest of which are the classical averaging schemes: Voigt average and Reuss average.<sup>4</sup> In the Voigt model, the constituents of the composite are assumed to be in parallel, and thus, are subjected to the same strain. The effective modulus is given by

$$E_c = E_p \phi + E_m(1 - \phi) \quad (5)$$

where  $E_c$ ,  $E_p$ , and  $E_m$  are the Young’s modulus of the composite, particle (filler), and the matrix, respectively, and  $\phi$  is the volume fraction of the filler.

In the Reuss average, the constituents of the composite are subjected to the same stress and the effective modulus is given by

$$\frac{1}{E_c} = \frac{\phi}{E_p} + \frac{(1 - \phi)}{E_m} \quad (6)$$

Hashin and Shtrikman<sup>5,6</sup> developed models based on macroscopical isotropy and quasi-homogeneity of the composite, where the shape of the reinforcement is not a limiting factor. The model initially assumes a homogeneous and isotropic reference material in which the constituents are dispersed. Depending on whether the stiffness of the reference material is more or less than that of the reinforcement, the upper and lower bounds are calculated as:

$$K_c^u = K_p + \frac{1 - \phi}{\frac{1}{K_m - K_p} + \frac{3\phi}{(3K_p + 4G_p)}} \quad (7)$$

$$K_c^l = K_m + \frac{\phi}{\frac{1}{K_p - K_m} + \frac{3(1 - \phi)}{(3K_m + 4G_m)}} \quad (8)$$

$$G_c^u = G_p + \frac{1 - \phi}{\frac{1}{G_m - G_p} + \frac{6\phi(K_p + 2G_p)}{5G_p(3K_p + 4G_p)}} \quad (9)$$

$$G_c^l = G_m + \frac{\phi}{\frac{1}{G_p - G_m} + \frac{6(1 - \phi)(K_m + 2G_m)}{5G_m(3K_m + 4G_m)}} \quad (10)$$

where  $K_p$  is the bulk modulus of the filler,  $G_p$  is the shear modulus of the filler,  $K_m$  is the bulk modulus of the matrix,  $G_m$  is the shear modulus of the matrix,  $K_c$  is the bulk modulus of the composite,  $G_c$  is the shear modulus of the composite, and superscripts “u” and “l” refer to the upper and lower bounds, respectively. These bounds are of practical value for phase stiffness mutual ratios up to about 10.<sup>6</sup>

**Coefficient of Thermal Expansion**

The rule of mixtures serves as the first-order approximation to the overall calculation of the coefficient of thermal expansion of the composite.<sup>7</sup> This can be expressed as

$$\alpha_c = \alpha_p \phi + \alpha_m(1 - \phi) \quad (11)$$

where  $\alpha_c$ ,  $\alpha_m$ , and  $\alpha_p$  represent the CTEs of the composite, the matrix, and the particle (filler), respectively, and  $\phi$  is the volume fraction of the filler.

Turner developed a model that takes into account the mechanical interaction between differ-

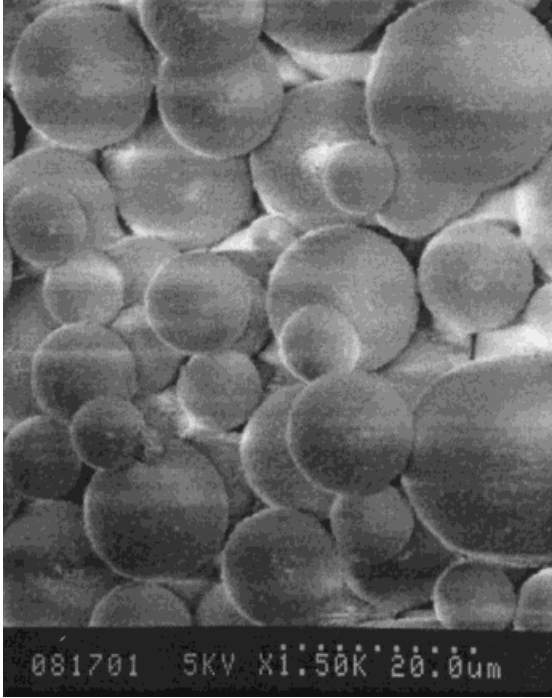


Figure 1 SEM micrograph of silica.

ent materials in the composite.<sup>8</sup> Based on the assumption that all phases in the composite have the same dimension change with temperature, he derived a relationship that is expressed as

$$\alpha_c = \frac{(1 - \phi)K_m\alpha_m + \phi K_p\alpha_p}{(1 - \phi)K_m + \phi K_p} \quad (12)$$

Based on thermoelastic principles, Schapery<sup>9</sup> developed a model to predict the upper and lower bounds of the CTE of a composite. The two bounds are given by:

$$\alpha_c^l = \alpha_m + \frac{K_p}{K_c^u} \frac{(K_m - K_c^u)(\alpha_p - \alpha_m)}{(K_m - K_p)} \quad (13)$$

$$\alpha_c^u = \alpha_m + \frac{K_p}{K_c^l} \frac{(K_m - K_c^l)(\alpha_p - \alpha_m)}{(K_m - K_p)} \quad (14)$$

where subscripts “u” and “l” refer to the upper and lower bounds, respectively. It can be seen that the upper and lower bounds as calculated from the Hashin-Shtrikman model are used to calculate the lower and upper bounds in the Schapery model.

## EXPERIMENTAL

### Materials

The epoxy resin used for the study was 3,4-epoxy cyclohexyl methyl-3,4-epoxy cyclohexyl caboxylate, manufactured by Union Carbide. The hardener used was hexahydro-4-methylphthalic anhydride from Aldrich Chemical Company. The catalyst used for curing was Iron (III) acetyl acetonate, also from Aldrich Chemical Company. All the above chemicals were used as received. The above system was chosen because of its low viscosity. The fillers used were silica-coated aluminum nitride (SCAN) from Dow Chemical Company, alumina from Showa Denko, and silica from Nippon Chemicals. A titanate coupling agent, tetra (2,2 diallyloxymethyl) butyl di (ditridecyl) phosphito titanate from Kenrich Petrochemicals, was used to treat the silica and alumina surfaces. The average particle size of the fillers used was 12–15 μm. SCAN was irregular in shape, alumina was close to spherical, and silica had a perfect spherical shape. Figures 1, 2, and 3 are typical SEM micrographs of silica, alumina, SCAN, respectively.

### Sample Preparation

A specified quantity of the epoxy resin and hardener were mixed thoroughly before the catalyst

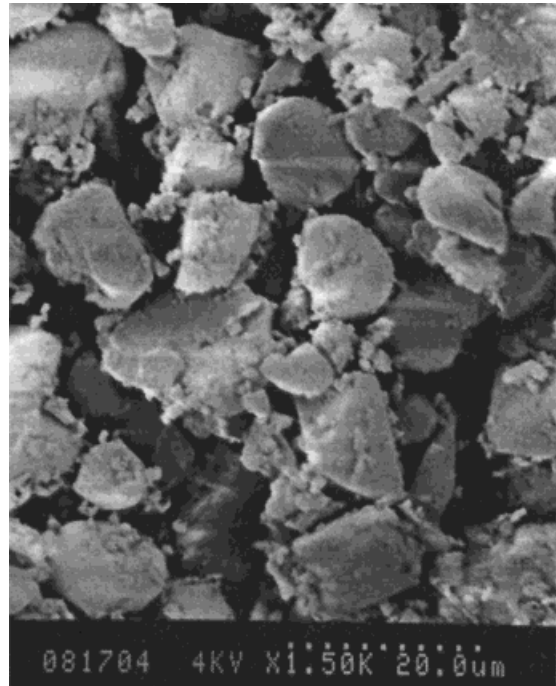
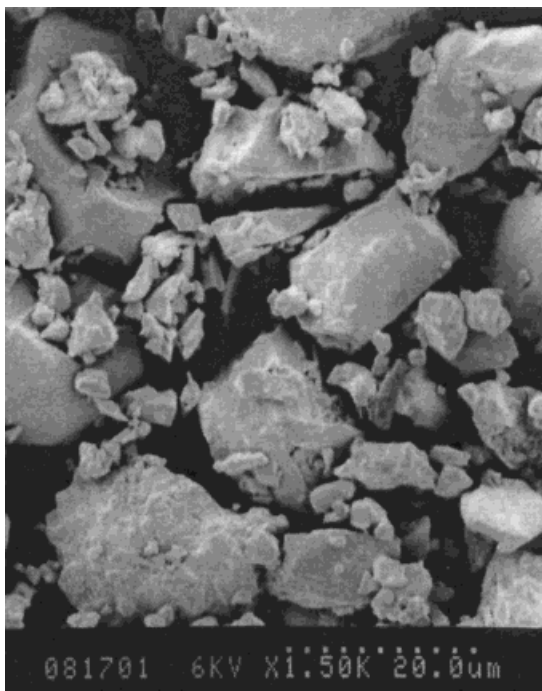


Figure 2 SEM micrograph of alumina.



**Figure 3** SEM micrograph of SCAN.

was added. This mixture was then stirred for about 3 h until the catalyst was fully dispersed. The titanate coupling agent was then added to the mixture. The amount of titanate used was 1% by weight of the filler. A commercial Waring blender was used to mix the filler with the above resin/hardener mixture. The mixture was stirred under high shear for about 30 min with intermittent pulsing to prevent the mixture from getting heated. After mixing, the samples were placed in a vacuum oven for about 1 h to remove entrapped air in the samples. These formulations were stored in a freezer at  $-40^{\circ}\text{C}$  when not in use. The samples were cured in 1.5-inch diameter aluminum pans. These pans were placed in a convective oven and heated to  $250^{\circ}\text{C}$  at a rate of  $3^{\circ}\text{C}/\text{min}$ .

The samples were held at this temperature for another 15 min. The cured samples were then cooled down to room temperature and machined into required dimensions using a diamond saw.

## Characterization

### Thermal Conductivity

The thermal conductivity measurements were made on a Holometrix TCA-200 guarded heat flow meter. These tests comply with ASTM F433, E1530 standard methods for determining the thermal conductivity. The cured samples were machined into squares having dimensions of  $1'' \times 1''$ . These machined samples were used for thermal conductivity measurements. Upon reaching thermal equilibrium, output data from the test were read on a digital display and thermal conductivity values were then computed using a utility software program. The conductivity was measured at a mean sample temperature of  $70^{\circ}\text{C}$ . The reported values are the averages of two measurements per sample.

### Coefficient of Thermal Expansion

CTE measurements of the cured samples were performed on a Thermal Mechanical Analyzer (TMA) (TA Instruments, Model 2940) using an expansion probe. These samples had a size of  $4 \times 4 \times 2$  mm. The samples were mounted on the TMA and heated to  $250^{\circ}\text{C}$  at a heating rate of  $10^{\circ}\text{C}/\text{min}$ . The coefficient of thermal expansion was determined from the slope of the plot between thermal expansion and temperature. The CTE was measured for two different samples with the same composition, and the average value is reported.

### Modulus of Elasticity

A Dynamic Mechanical Analyzer (DMA) (TA Instruments, Model 2980) was used to determine

**Table I** Material Properties of the Resin and Fillers

Material	Epoxy	Silica	SCAN	Alumina
Thermal conductivity (W/mK)	0.195	1.5	220	36
CTE (PPM/ $^{\circ}\text{C}$ )	88	0.5	4.4	6.6
Young's modulus (GPa)	2.25	73	330	385
Poisson's ratio	0.19	0.19	0.25	0.24
Shear modulus (GPa)	0.8	31	132	155
Bulk modulus (GPa)	3.75	39	220	247
Density (g/cc)	1.1	2.2	3.26	3.98

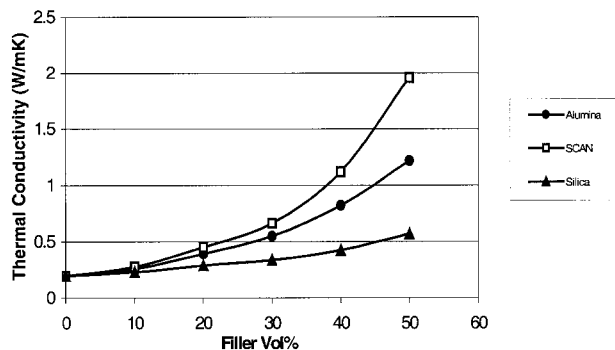


Figure 4 Thermal conductivity as a function of volume loading for different fillers.

the storage moduli of the samples. These samples were in the form of strips having dimensions of about  $32 \times 11 \times 3$  mm. A single cantilever mode under 1-Hz sinusoidal strain loading was used for the tests. The specimen was mounted on the DMA and heated from room temperature to  $300^\circ\text{C}$  at a heating rate of  $3^\circ\text{C}/\text{min}$ . The storage modulus ( $E'$ ) was calculated using a preinstalled software program. The data reported is the modulus at  $25^\circ\text{C}$ , and is the average of measurements on two different samples with the same composition.

Adhesion Strength

Adhesion strength of the epoxy to silica and alumina interfaces was accomplished in a shear mode using a bond tester (Model 550-100K, Royce Instruments). To test the adhesion between the resin and silica interface,  $80 \times 80$  mil  $\text{SiO}_2$  passivated silicon die were used. A thin layer of the epoxy resin was applied to the die, and these were then placed on a  $\text{SiO}_2$  passivated silicon sub-

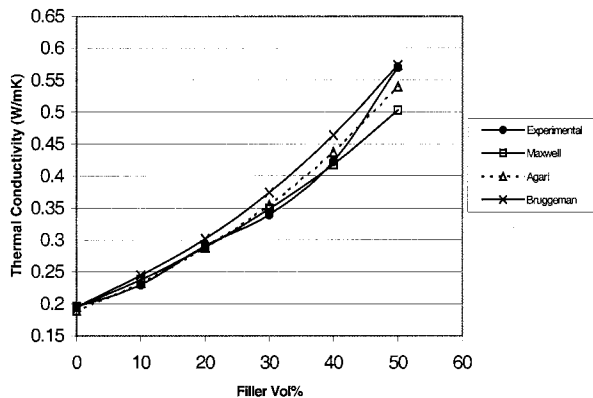


Figure 5 Comparison of thermal conductivity of silica-filled composites with theoretical predictions.

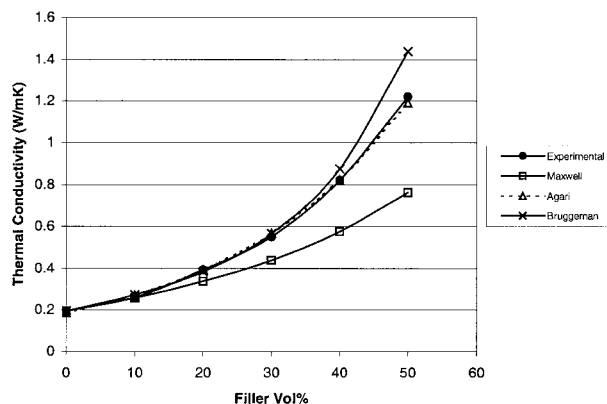


Figure 6 Comparison of thermal conductivity of alumina-filled composites with theoretical predictions.

strate. The epoxy resin was then cured under the same conditions as specified earlier. For measuring the adhesion strength between the resin and alumina interface, similar die ( $80 \times 80$  mil  $\text{SiO}_2$  passivated silicon) were used on an alumina substrate. In either case, adhesion measurements were done on 20 die, and the average strength was obtained.

RESULTS AND DISCUSSION

In the results presented below, the filler loading is always expressed in volume percent unless stated otherwise. The following relation was used to determine the volume fraction of the filler for a given weight fraction.

$$\phi = \frac{W}{W + (1 - W) \frac{\rho_f}{\rho_m}} \tag{15}$$

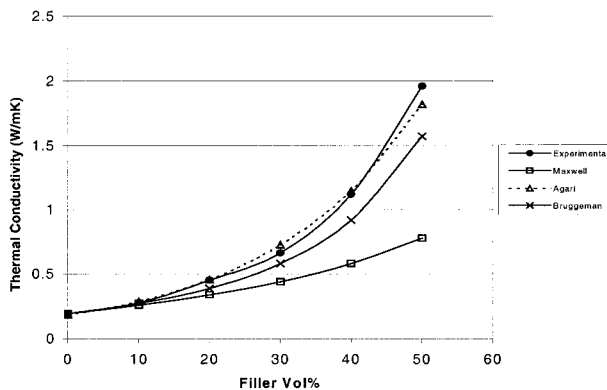


Figure 7 Comparison of thermal conductivity of SCAN-filled composites with theoretical predictions.

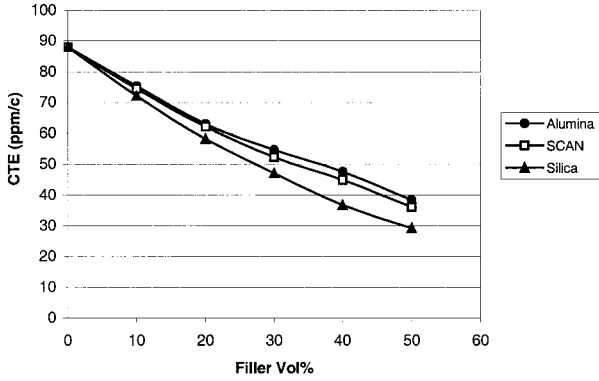


Figure 8 CTE as a function of volume loading for different fillers.

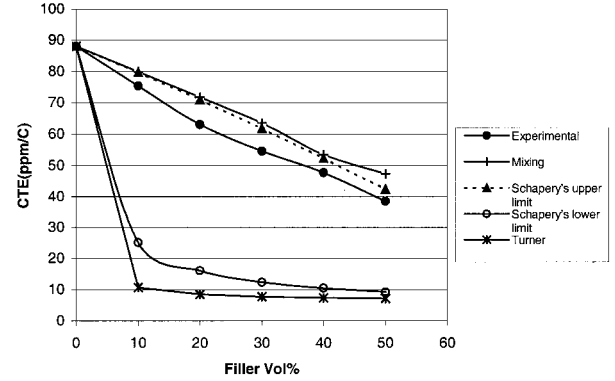


Figure 10 Comparison of CTE of alumina-filled composites with theoretical predictions.

where  $\phi$  is the volume fraction,  $W$  is the weight fraction,  $\rho_f$  is the density of the filler, and  $\rho_m$  is the density of the matrix.

Table I lists the material properties of the resin and filler that were used to estimate the composite properties. The properties of the resin were determined experimentally, while that of the fillers were obtained from the vendors.

### Thermal Conductivity

The thermal conductivity as a function of filler loading is shown in Figure 4. It shows a superlinear increase with increase in the filler loading. For any given filler loading, SCAN filled samples have the highest conductivity, while silica-filled formulations have the lowest conductivity. The low conductivity of silica-filled formulations is due to the low thermal conductivity of fused silica (1.5 W/mK). A conductivity of 1.96 W/mK was achieved with a 50% SCAN. This is about 10

times the intrinsic conductivity of the polymer. Figures 5, 6, and 7 show the comparison between theoretical models and experimental data for the thermal conductivity of silica, alumina, and SCAN-filled systems. For silica-filled systems, both the Maxwell model and the Agari and Uno model provide a better estimate of thermal conductivity compared to the Bruggeman model. For alumina- and SCAN-filled systems, the Agari and Uno model fits the data fairly well. The constants  $C_1$  and  $C_2$  in the Agari and Uno model are determined by curve fitting of the experimental data, and hence, this model represents the data better than other models.

### Coefficient of Thermal Expansion

The CTE before glass transition temperature ( $T_g$ ) of the cured resin without any filler is about 88 ppm/°C. From Figure 8 it can be seen that with an increase in the filler content, the CTE decreases. For any given filler loading, silica-filled samples

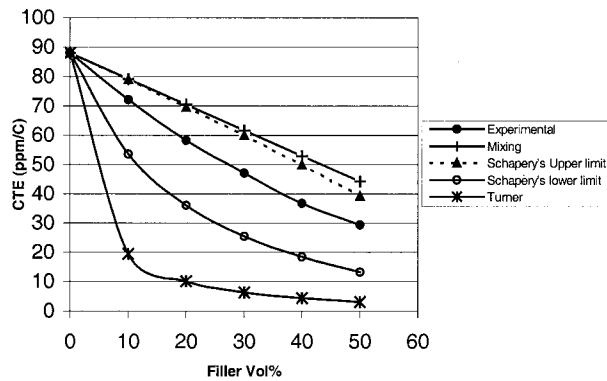


Figure 9 Comparison of CTE of silica-filled composites with theoretical predictions.

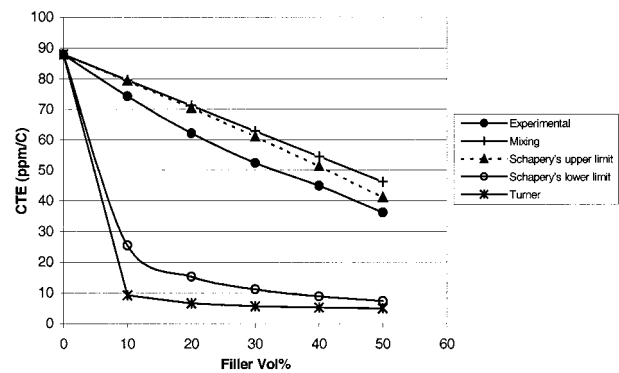
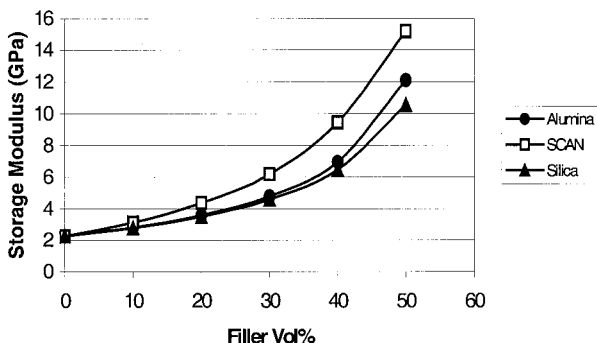


Figure 11 Comparison of CTE of SCAN-filled composites with theoretical predictions.



**Figure 12** Modulus as a function of volume loading for different fillers.

have the lowest CTE, and alumina-filled samples have the highest CTE. This can be explained as follows. The intrinsic CTEs of the fillers in the order of increasing magnitude is silica < SCAN < alumina. Therefore, for any given filler loading, the composite CTEs follow the same order as that of the fillers. Figures 9, 10, and 11 show the comparison between experimental data and theoretical models for the CTE of silica; alumina-, and SCAN-filled systems. It can be seen that for all the systems the CTE obtained lies in between Schapery's upper and lower bounds. The deviation from experimental data is smaller for Schapery's upper bound than the lower bound.

**Modulus of Elasticity**

Figure 12 shows the plot of storage modulus as a function of filler loading for different fillers. The increase in the modulus with filler loading shows the same super linear trend as observed with thermal conductivity. For any given filler loading,

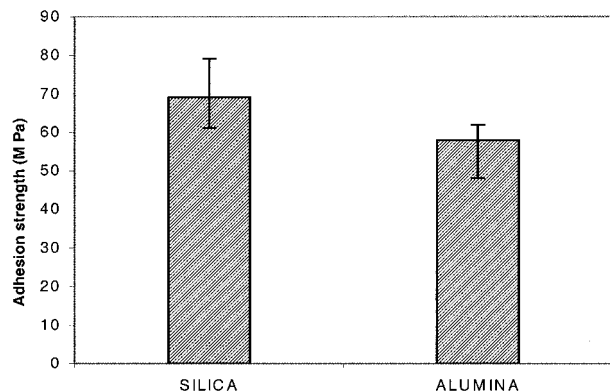


**Figure 13** Adhesion strength between the silica and alumina interfaces with the epoxy.

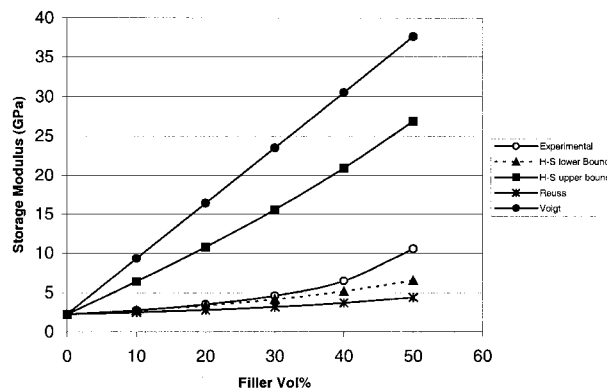


**Figure 14** Comparison of modulus of silica-filled composites with theoretical predictions.

SCAN filled samples have the highest modulus. Although the intrinsic modulus of alumina is the highest of all the fillers, alumina-filled samples do not have higher moduli than those with SCAN. This can be attributed to the greater degree of irregularity in the shape of SCAN particles when compared to alumina. These results confirm the theoretical predictions of Wu.<sup>10</sup> Another possible reason to explain the higher modulus of SCAN-filled composites is better adhesion between the silica interface of SCAN and epoxy than the adhesion between alumina interface and epoxy. Interfacial adhesion between silica and alumina surfaces with epoxy was studied to justify the explanation. Figure 13 shows the results of the adhesion strength of epoxy to silica and alumina interfaces as determined from die shear measurements. It can be seen that the adhesion strength between the epoxy and silica interface is higher than that between the epoxy and alumina interface. Good interfacial adhesion between the resin and the filler results in better reinforcement, and hence, a higher modulus. The predicted values of

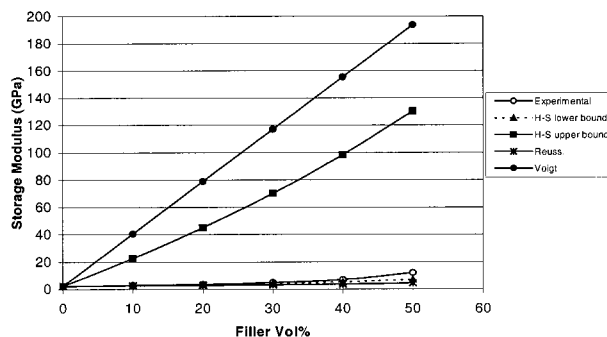


**Figure 15** Comparison of modulus of alumina-filled composites with theoretical predictions.

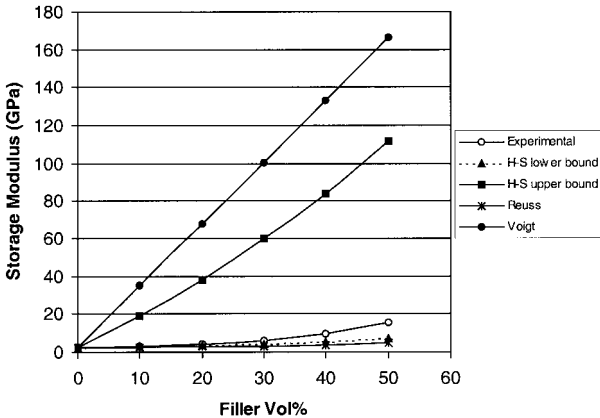


**Figure 16** Comparison of modulus of SCAN-filled composites with theoretical predictions.

elastic modulus using theoretical equations are compared with experimental data for silica-, alumina-, and SCAN-filled composites in Figures 14, 15, and 16 respectively. The modulus of all the composites lie in between the Hashin-Shtrikman bounds. It is seen that the Hashin-Shtrikman lower bound fits the data well at low concentrations of the filler, after which it begins to deviate from the measured values.

## CONCLUSIONS

The thermal conductivity of alumina and SCAN filled composites is much higher than those filled with silica. At a volume loading of 50%, the ther-

mal conductivity of SCAN-filled composites is 10 times the intrinsic thermal conductivity of the epoxy resin. It was found that the Agari and Uno model fits the thermal conductivity data fairly well. The study on the elastic modulus showed that adhesion between the resin and filler, and the shape of the filler particles play an important role in determining the composite modulus. SCAN-filled composites have the highest modulus for any given filler loading. The Hashin-Shtrikman lower bound provides a good estimate of the composite modulus at low filler loadings. Silica-filled composites have the lowest CTE at any given filler loading, and the CTEs of all the composites lie in between Schapery's upper and lower bounds.

## REFERENCES

1. Maxwell, J. C. A Treatise on Electricity and Magnetism; Dover: New York, 1954, 3rd ed.
2. Sundstrom, D. W.; Lee, Y.-D. *J Appl Polym Sci* 1972, 16, 3159.
3. Agari, Y.; Uno, T. *J Appl Polym Sci* 1986, 32, 5705.
4. Ahzi, S.; Parks, D. M.; Argon, A. S. *AMD ASME* 1995, 203, 31.
5. Hashin, Z.; Shtrikman, S. *J Mech Phys Solids* 1963, 11, 127.
6. Hashin, Z. *J Appl Mech* 1983, 50, 481.
7. Orrhede, M.; Tolani, R.; Salama, K. *Res Nondestr Eval* 1996, 8, 23.
8. Tokunaga, Y.; et al. *ASME* 1992, 613.
9. Schapery, R. A. *J Comp Mater* 1968, 2, 380.
10. Wu, T. T. *Int J Solids Struct* 1966, 2, 1.